Analytical Design of Sensor Configuration for EEG *

Chandra Vaidyanathan and Kevin M. Buckley
Department of Electrical Engineering
University of Minnesota
Minneapolis, MN 55455

ABSTRACT

This paper addresses the problem of electrode configuration design for recording electroencephalogram (EEG) signals. The standard 10 − 20 configuration, which is widely employed, uses 21 sensors and has been demonstrated to be inadequate. EEG researchers,therefore, have been using more sensors. However, no theoretical studies have been conducted on selecting the number of sensors and for placement of the electrodes. In this paper we present a technique based on finite sum approximation to a continuous potential function on the surface of a sphere. We then borrow techniques from sampling theory to select the number of sensors and a suggest a strategy for placing them.

1 Introduction

Electroencephalogram (EEG) signals are potentials measured at discrete locations, by an array of electrodes, on the surface of the human scalp. These represent the underlying neuronal activity of the brain. The most commonly used electrode configuration is the 10 − 20 system [1]. This 21 sensor configuration was designed to cover different lobes of the brain. However, it is realized that for accurate evoked potential localization this configuration is inadequate, and researchers have been using up to about 128 sensors. The need for additional electrodes were addressed by Gevins [2] for event related potential fields. Sampling densities were determined experimentally by measuring the spectral power at different spatial frequencies and electrode spacing of 2cm-2.5cm was suggested to prevent spatial aliasing.

New standards for electrode placement need to be introduced to replace the 10 − 20 system. While the number of electrodes needed and their placement depends on the experiment under consideration, a general framework is desirable. We present here an analytical tool to help in selecting the number of electrodes. Conditions on the electrode configuration are then presented.

Our first approach is based on sampling the continuous potential function over the aperture[1], which is the scalp in this case. We assume that the scalp can be modeled as a hemispherical surface (see figure 1). This assumption is consistent with the three/four sphere model commonly used in the EEG literature [3]. The spherical model gives us an analytical formulation in terms of the spherical harmonics for the potential function on surface of a sphere. We use this model to study the properties of potential on the scalp, and determine the number of spatial sampling points we need to represent this function within a certain degree of approximation.

To maintain generality we present the theory for a general potential function on a hemispherical surface with the aid of generalized Green's functions [4]. We then discuss specifically the problem of EEG potentials. Since the sources are at a distance (brain) from the aperture (scalp), the spatial energy is shown to fall off exponentially. We use an equivalent double layer on the cortex to determine the dimensionality of the observation. For simulations, we use the four sphere model, since it incorporates different layers in the propagation of the potential. A more general approach is then suggested for finding the number of electrodes needed. This second approach uses a source representation subspace approach which is independent of the geometry of the problem and is verified by comparison to the first approach.

2 Potential function on a hemisphere

The potential function on the surface of the hemisphere can be expressed as

$$V_H(\theta,\phi) = 2\sum_{n=0}^{\infty}\{a_{n,0}Y_{n,0}(\theta) + \sum_{m=1}^{n} a_{n,m}Y^0_{n,m}(\theta,\phi)\}, \quad (1)$$

where $(0 < \theta < \pi)$ and $(0 < \phi < \pi)$ are the elevation and azimuth in spherical coordinate system, respectively and $Y_{n,0}(\theta)$ and $Y^0_{n,m}(\theta,\phi)$ are the spherical harmonics[2] of order n defined as

$$Y_{n,0}(\theta) \doteq \sqrt{\frac{(2n+1)}{4\pi}}P_n(\cos\theta), \quad (n = 0, 1, \cdots), \quad (2)$$

*This work was supported in part by *ONR* under contract number N00014-90-J-1049 and NSF under contract number MIP-9057071.

[1]The spatial extent over which the observation is gathered is called the aperture.

[2]The spherical harmonics are the eigenfunctions of the Laplace's equation in spherical coordinates [4].

$$Y^0_{n,m}(\theta,\phi) \doteq \sqrt{\frac{(2n+1)}{2\pi}\frac{(n-m)!}{(n+m)!}} P^m_n(\cos\theta)\cos m\phi. \tag{3}$$

In these expressions P_n and P^m_n are the Legendre and the associated Legendre polynomial of order n, respectively.

Note that, since the domain is a hemispherical surface the above representation is derived from the spherical harmonic series for a spherical surface [4] by assuming an even extension over $(-\pi < \phi < 0)$. The coefficients in equation (1) can be determined from the relations

$$a_{n,0} = \int\int_S V_H(\theta,\phi) Y_{n,0}(\theta) dS, \qquad (n = 0, 1, \cdots), \tag{4}$$

$$a_{n,m} = \int\int_S V(\theta,\phi) Y^0_{nm}(\theta,\phi) dS, \quad (m = 1, 2, \cdots, n), \tag{5}$$

where

$$\int\int_S dS \doteq \int_0^\pi d\phi \int_0^\pi \sin\theta d\theta. \tag{6}$$

is the surface integral.

2.1 Dimensionality

Since we wish to restrict the dimensionality of the problem by truncating the infinite series in equation (1) to a finite sum, we need to examine the rate of decay of the coefficients in this equation. A practical measure is to approximate the function with a prescribed mean square error, i.e. find N such that

$$||V_H(\theta,\phi) - \sum_{n=0}^{N}[a_{n,0}Y_{n,0}(\theta) + \sum_{m=1}^{n} a_{n,m}Y^0_{n,m}(\theta,\phi)]||^2 \leq \epsilon_N. \tag{7}$$

We proceed by identifying the integral kernels associated with the potential function. The generalized Green's function [4, pp. 363-378] are the solutions to a given partial differential equation with a given set of boundary conditions. We can find the dimensionality of the problem by approximating this function by a finite set of functions within a specified mean square error. The generalized Green's function is the integration kernel, $\mathcal{G}(\vec{\chi},\vec{\chi}')$, for the eigenfunctions involving the potential function on a hemispherical surface and is given by

$$\mathcal{G}_H(\vec{\chi},\vec{\chi}') = -\frac{1}{2\pi}[1 + \ln\sin\frac{\gamma}{2} + \ln\sin\frac{\gamma'}{2}], \tag{8}$$

where $\vec{\chi} : (r,\theta,\phi)$ and $\vec{\chi}' : (r,\theta',\phi')$ are two points on the surface of the hemisphere and

$$\cos\gamma = \cos\theta\cos\theta' + \sin\theta\sin\theta'\cos(\phi-\phi'), \tag{9}$$

$$\cos\gamma' = \cos\theta\cos\theta' + \sin\theta\sin\theta'\cos(\phi+\phi'). \tag{10}$$

The kernel, $\mathcal{G}(\vec{\chi},\vec{\chi}')$, is positive definite, symmetric and has points of singularity at $\gamma = 0$ & $\gamma' = 0$. However, although the kernel becomes infinite at a some point a weaker form of Mercer's theorem,

$$\mathcal{G}_H(\chi,\chi') = \underset{N\to\infty}{\text{l.i.m}} \sum_{n=1}^{N} 2\lambda_n[Y_{n,0}(\theta)Y_{n,0}(\theta') + \sum_m Y^0_{n,m}(\theta,\phi)Y^0_{n,m}(\theta',\phi')], \tag{11}$$

holds. Note that, since the eigenvalues are $(n+1)$ fold degenerate, for each λ_n we have $(n+1)$ terms in the above summation. Using the addition theorem for spherical harmonics [5], we can simplify equation (11) to

$$\mathcal{G}_H(\chi,\chi') = \underset{N\to\infty}{\text{l.i.m}} \sum_{n=1}^{N} c_{H,n}\sqrt{n+1}[Y_{n,0}(\gamma)+Y_{n,0}(\gamma')], \tag{12}$$

where $\sqrt{n+1}$ is a normalization constant and

$$c_{H,n} \doteq \frac{1}{\sqrt{4\pi}}\frac{(2n+1)}{n(n+1)^{1.5}}. \tag{13}$$

We can, therefore, find an N, such that for a given mean square error, ϵ_N,

$$1 - \sum_{n=N+1}^{\infty} c^2_{H,n} / \sum_{n=1}^{\infty} c^2_{H,n} = \frac{1}{(N+1)^2} \leq \epsilon_N. \tag{14}$$

Figure 2 shows the plot of the error as we increase N. Observe that there is no apparent elbowing of the curve to select N. Therefore, we specify a value of ϵ_N and select corresponding N. Note that for each n we need $(n+1)$ coefficients. Therefore, the number of coefficients we need to estimate in (1) is

$$D_H = \sum_{n=0}^{N}(n+1) = \frac{(N+1)(N+2)}{2}. \tag{15}$$

This is the total dimensionality of our problem. This implies we need a total of D_H sensors to reconstruct the potential function on the surface to a given degree of approximation, ϵ_N. Note that we have considered the most general potential function. The convergence of the error is rather slow for this case. By further restricting the property of the potential function we can achieve further reduction in D.

2.2 Number of electrodes

The analysis in the previous section indicates rather slow decay for the spherical harmonic coefficients. However, for the EEG problem, the sources are at a distance from the surface of the sphere. In this case, the decay is faster than the earlier two criteria. Also, since the potentials propagate through different layers it further reduces the dimensionality of the observation.

The potential due to any source can be modeled by a double layer enclosing the source. Therefore, we model the source as a equivalent double layer on a concentric sphere of radius r_0 $(< r)$. r_0 is the radius of the smallest sphere enclosing all the sources. Here we

chose this sphere to be the cortical surface. Since we treat the potential function to be an even function in the variable ϕ, our equivalent dipole layer is modeled as an even function. The double layer is treated here as a collection of point dipoles with arbitrary orientation distributed over the surface.

Consider a point dipole located at point $\vec{s}_0$: (r_0, θ_0, ϕ_0) at the cortex. The potential at $\vec{\chi}$ due to the dipole with arbitrary orientation is represented by the $\vec{g}^T(\vec{s}_0, \vec{\chi})\vec{m}(\vec{s}_0)$. $\vec{m}(\vec{s}_0)$ is the dipole moment and $\vec{g}(\cdot)$ is the transfer function for the potential at $\vec{\chi}$ due to a dipole at $\vec{s}_0$. We consider dipoles located at points $\vec{s}_0 = (r_0, \theta_0, \phi_0)$ and $\vec{s'}_0 = (r_0, \theta_0, -\phi_0)$ with the same moment $\vec{m}(\vec{s}_0)$. The potential at $\vec{\chi}$ due to these dipoles is then given by $[\vec{g}(\vec{s}_0, \vec{\chi}) + \vec{g}(\vec{s'}_0, \vec{\chi})]^T \vec{m}(\vec{s}_0)$. The covariance function of the observation at the surface of the sphere for a layer of such dipoles is then given by

$$\begin{aligned}\mathbf{K}_H(\vec{\chi}, \vec{\chi'}) &= \iint_{S_0} W(\vec{s}_0)[\vec{g}(\vec{s}_0, \vec{\chi}) + \vec{g}(\vec{s'}_0, \vec{\chi})] \\ &\qquad \mathbf{M}(\vec{s}_0)[\vec{g}(\vec{s}_0, \vec{\chi'}) + \vec{g}(\vec{s'}_0, \vec{\chi'})]^T d\mathcal{S}_0 \\ &= C \sum_{n=1}^{\infty} \mu_{H,n}^2 \sqrt{n+1}[Y_{n,0}(\gamma) + Y_{n,0}(\gamma')], \quad (16)\end{aligned}$$

where $\mathbf{M}(\vec{s}_0) = \mathcal{E}[\vec{m}(\vec{s}_0)\vec{m}^T(\vec{s}_0)]$, $W(\vec{s}_0)$ is a weighting function and

$$\mu_{H,n}^2 = w_n^2 (\frac{r_0}{r})^{2n} \frac{2n^2 + n(n+1)}{(2n+1)\sqrt{(n+1)}}. \quad (17)$$

The above expression can be derived using results from [6]. w_n is a weight which depends on conductivities and radii of different layers. $\mathbf{M}(\vec{s}_0)$ is assumed to be the identity matrix and the dipole layer is assumed to have uniform distribution over the entire sphere, i.e. $W(\vec{s}_0) = 1$. The covariance function is an integral kernel for spherical harmonics. We could chose N such that

$$1 - \sum_{n=N+1}^{\infty} \mu_{H,n}^2 / \sum_{n=1}^{\infty} \mu_{H,n}^2 \leq \eta_N \quad (18)$$

Figure 3 shows the plot of the error, η_N as we increase N. The four sphere model parameters were used to generate this plot. The radii were chosen to be $r = 0.088m$ (scull) and $r_0 = 0.078m$ (cortex).

For example, for $\eta_N = 20dB$ and $30dB$ we have $N = 8$ and 14, respectively. For the examples we considered, we have $D_H = 45$ and 130, respectively. Typically, resolution requirements and noise variance can dictate the value of N. A resolution requirement could be the number of multipole components we need to estimate. ϵ_N is usually chosen to above the noise floor, since the signal buried below the noise level cannot be observed. The noise level also would give an upper bound on the number of multipole coefficients we could estimate. The noise is assumed to be mostly due to instrumental errors (impedance of devices, electrode contacts, proper electrode placement etc.). If the input impedance of a commercial differential amplifier is of the order $1M\Omega$ and the inter-electrode impedance is of the order $10K\Omega$, then 99% of the scalp potential is available at the output of the amplifier [7]. Here it is assumed that the signal to noise ratios (SNR) are higher and examples are presented for SNR = $20dB$ (and $30dB$), i.e. 99.90% (or 99.97%) of the signal is captured by the recording devices.

2.3 Numerical algorithm to determine the number of sensors

The above study indicates a need for a large number of sensors. We note that in actual EEG the dimensionality could be much lower due to various factors not considered in the above study. The equivalent layer typically will not have constant magnitude over the entire sphere. However, this assumption gives an upper bound on the number of sensors required. For weighting functions, $W(\vec{s}_0)$, which taper off, the dimensionality is much less. Selection of $W(\vec{s}_0)$ is application dependent is not addressed here.

The advantage of a numerical technique over the analysis presented earlier is that it is independent of the spherical assumption. We assume we have a forward model for a dipole source for the geometry of the problem. An FEM based model could be used for this setup. The aperture is filled with a large number of electrodes (K) and the covariance matrix (16) is then evaluated for a dipole layer with a given weight function. The dipole layer is modeled as a dense set of point dipoles ($M > K$) over a closed surface, S_0, enclosing the sources. An eigenvalue decomposition is then performed on the covariance matrix. The behavior of the eigenvalues should then indicate the dimension of the observation [8] (i.e. the number of electrodes to select).

The algorithm is as follows,

1. Define the $K \times K$ source sample covariance matrix

$$\mathbf{R}_s = \iint_{S_0} W(\vec{s}_0)\mathbf{G}(\vec{s}_0)\mathbf{G}^T(\vec{s}_0) d\mathcal{S}_0, \quad (19)$$

where

$$\mathbf{G}(\vec{s}_0) = \begin{bmatrix} \vec{g}^T(\vec{s}_0, \vec{\chi}_1) \\ \vec{g}^T(\vec{s}_0, \vec{\chi}_2) \\ \vdots \\ \vec{g}^T(\vec{s}_0, \vec{\chi}_K) \end{bmatrix}. \quad (20)$$

2. Compute the singular value decomposition (SVD) on the stacked matrix

$$[\sqrt{W(\vec{s}_0)}\mathbf{G}(\vec{s}_0), \cdots, \sqrt{W(\vec{s}_{M-1})}\mathbf{G}(\vec{s}_{M-1})] = \mathbf{U}\mathbf{\Sigma}\mathbf{V}^T, \quad (21)$$

where $\mathbf{\Sigma} = diag(\sigma_n^2)$ and $\mathbf{U} = [\vec{u}_1, \cdots, \vec{u}_K]$. $\mathbf{R}_s$ is then represented using an orthogonal basis

$$\mathbf{R}_s = \sum_{n=1}^{K} \sigma_n^2 \vec{u}_n \vec{u}_n^T, \quad (22)$$

and σ_n^2 are the eigenvalues.

3. The dimension of the matrix can be determined from σ_n^2. We could then select the number of electrodes, N, based on

$$1 - \sum_{n=N+1}^{K} \sigma_n^2 / \sum_{n=1}^{K} \sigma_n^2 \leq \eta_N \qquad (23)$$

Figure (4) shows the plot of (23). The solid line represents the energy not represented for the whole sphere case. The four sphere model was used to generate the forward model. 900 sensors were distributed evenly over the hemisphere and about 3000 dipoles were used to generate the matrix in equation (21). For the $20dB$ ($30dB$) point, the number of sensors were 43 (134). Notice the close match with those computed in section 2.2.

3 Sampling theorem

We next derive a sampling theorem for the potential functions on a hemisphere. We first identify the reproducing kernel of the potential function so that conditions on electrode placement can be stated. Since the dimension of the space is D, we can represent the potential function from D samples and an interpolation function is derived to reconstruct the continuous functions. We adapt the general approach outlined in [9] to the potential on a spherical surface problem. Truncating the series in equation (1), we obtain

$$V_{H,N}(\theta,\phi) = 2\sum_{n=0}^{N}\{a_{n,0}Y_{n,0}(\theta) + \sum_{m=1}^{n} a_{n,m}Y^0_{n,m}(\theta,\phi)\}. \qquad (24)$$

Substituting the values of the coefficients, $a_{n,0}$ and $a_{n,m}$, from equations (4) & (5), we get

$$V_{H,N}(\theta,\phi) = 2\int\!\!\int_{S'} V_{H,N}(\theta',\phi')\sum_{n=0}^{N}[Y_{n,0}(\theta)Y_{n,0}(\theta') + \sum_{m=1}^{n} Y^0_{n,m}(\theta,\phi)Y^0_{n,m}(\theta',\phi')]dS'. \qquad (25)$$

The terms in the summation can be simplified using addition theorems. Define

$$k_{H,N}(\vec{\chi},\vec{\chi}') = \frac{2}{\pi}\sum_{n=0}^{N}(2n+1)[P_n(\cos\gamma) + P_n(\cos\gamma')] \qquad (26)$$

Therefore,

$$V_{H,N}(\theta,\phi) = \int\!\!\int_{S'} V_{H,N}(\theta',\phi')k_{H,N}(\vec{\chi},\vec{\chi}')dS'. \qquad (27)$$

The function, $k_{H,N}(\vec{\chi},\vec{\chi}')$ is the reproducing kernel of the potential functions defined by (24) on the surface of a hemisphere. Choose spatial points $[\vec{\chi}_1,\vec{\chi}_2,\cdots,\vec{\chi}_{D_H}]$ such that the matrix $\mathbf{K}_{H,N}$ with elements

$$\mathbf{K}_{H,N}(n,m) = k_{H,N}(\vec{\chi}_n,\vec{\chi}_m) \qquad (28)$$

is nonsingular. An optimum electrode configuration is one for which the matrix $\mathbf{K}_{H,N}$ is diagonal. Such a sequence does not exist for this problem. Define

$$\begin{bmatrix} S_{H,1}(\theta,\phi) \\ S_{H,2}(\theta,\phi) \\ \vdots \\ S_{H,D_H}(\theta,\phi) \end{bmatrix} = \mathbf{K}^{-1}_{H,N}\begin{bmatrix} k_{H,N}(\vec{\chi}_1,\vec{\chi}) \\ k_{H,N}(\vec{\chi}_2,\vec{\chi}) \\ \vdots \\ k_{H,N}(\vec{\chi},\vec{\chi}) \end{bmatrix}. \qquad (29)$$

$S_{H,n}(\theta,\phi)$ and $k_{H,N}(\vec{\chi}_n,\vec{\chi})$ form a biorthogonal sequence[3]. We can now state the sampling theorem

$$V_{H,N}(\theta,\phi) = \sum_{n=1}^{D_H} V_{H,N}(\theta_n,\phi_n)S_{H,n}(\theta,\phi). \qquad (30)$$

$S_{H,n}(\theta,\phi)$ is the sampling sequence with the property

$$S_{H,n}(\theta_m,\phi_m) = \delta_{nm}. \qquad (31)$$

An optimum orthogonal electrode configuration based on the sampling kernel does not exist for this problem, i.e. $\mathbf{K}_{H,N}$ is not diagonal. We can only specify the constraint an electrode configuration should satisfy, i.e. $\mathbf{K}_{H,N}$ is nonsingular. However, it is possible to design an optimum electrode array for specific applications using optimization schemes.

4 Summary

We derive analytical expressions to determine the number of sensors needed to record EEG potential functions. The asusmption of a sperical geometry is made for this study. A numerical technique is then presented for more complex geometries. Finally we derive a sampling theorem for potential functions on a hemispherical surface. A condition on the placement of electrodes is then stated.

References

[1] R. Katznelson, "EEG recording, electrode placement and aspects of generator localization," in *Electric Fields of the Brain* (P. Nunez, ed.), Oxford Press, New York, 1981.

[2] A. Gevins, "Dynamic patters in multiple lead data," in *Event-Related Brain Potentials:Basic Issues and Applications* (J. Rohrbaugh, R. Parasuraman, and J. R. Johnson, eds.), vol. 2, pp. 44–56, 1989.

[3] B. N. Cuffin and D. Cohen, "Comparison of the magnetoencephalogram and electroencephalogram," *Electroencephalography and Clinical Neurophysiology*, pp. 132–149, 1979.

[4] R. Courant and D. Hilbert, *Methods of Mathematical Physics, part I.* Interscience Publishers Inc., New York, 1953.

[3] $\int_S S_{H,n}(\vec{\chi})k_{H,N}(\vec{\chi}_m,\vec{\chi})dS = \delta_{nm}$

[5] C. Vaidyanathan and K. M. Buckley, "A sampling theorem for EEG electrode configuration," submitted to *IEEE Transaction on Biomedical Engineering*, 1994.

[6] J. C. de Munck, P. C. M. Vijn, and F. H. L. da Silva, "A random dipole model for spontaneous brain activity," *IEEE Transactions on Biomedical Engineering*, vol. 39, no. 8, pp. 791–804, Aug. 1992.

[7] A. Kriss, "Recording technique," in *Evoked Potentials in Clinical Testing* (A. M. Halliday, ed.), pp. 1–56, Churchill Livigstone, New York, 1993.

[8] K. M. Buckley, "Spatial/spectral filtering with linearly constrained minimum variance beamformers," *IEEE Transactions on Acoustics, Speech, and Signal Processing*, vol. 35, no. 3, pp. 249–266, Mar. 1987.

[9] M. Z. Nashed and G. G. Walter, "General sampling theorems for functions in reproducing kernel hilbert spaces," *Mathematics of Control, Signals and Systems*, vol. 4, pp. 363–390, 1991.

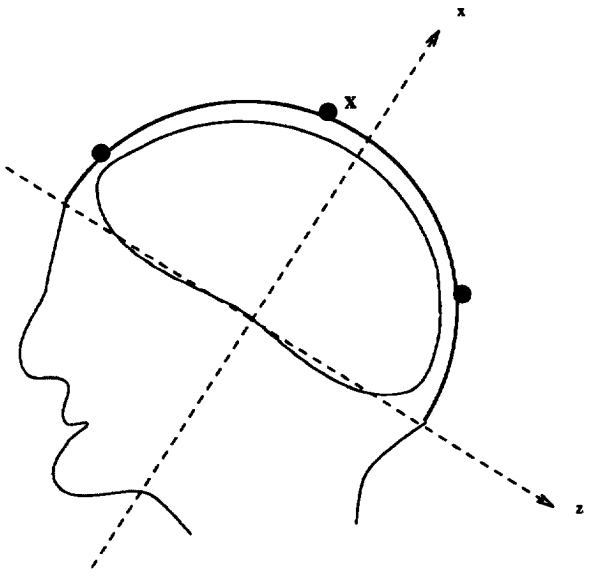

Figure 1: Figure to illustrate the head model.

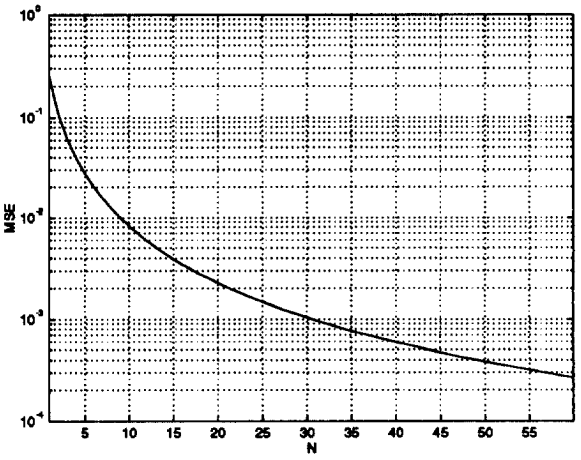

Figure 2: Plot of the error, $10log(\epsilon_N)$.

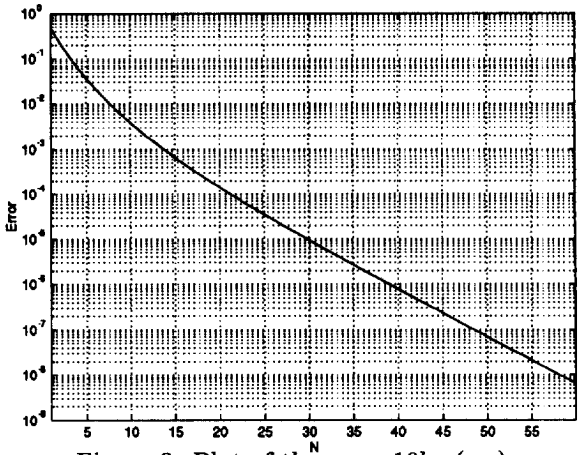

Figure 3: Plot of the error $10\log(\eta_N)$

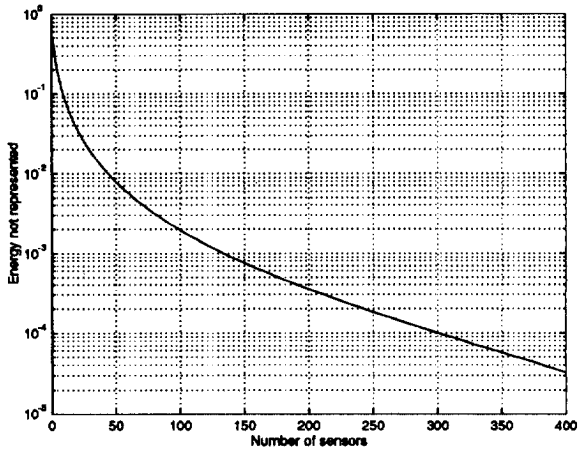

Figure 4: Plot of energy not represented versus number of sensors.